SURFACE AND INTERFACE ANALYSIS
Surf. Interface Anal. 2003; **35**: 593–603
Published online in Wiley InterScience (www.interscience.wiley.com). DOI: 10.1002/sia.1578

SIA

Glow discharge modelling: from basic understanding towards applications

Annemie Bogaerts,* Zhaoyang Chen and Renaat Gijbels

University of Antwerp, Department of Chemistry, Universiteitsplein 1, B-2610 Wilrijk-Antwerp, Belgium

Received 24 December 2002; Revised 25 February 2003; Accepted 25 February 2003

We have developed a comprehensive modelling network for glow discharge plasmas used for analytical spectroscopy in order to obtain better insight into the plasma characteristics that are desirable for good analytical practice. The modelling network consists of Monte-Carlo, fluid and collisional-radiative models, as well as a heat transfer model and a computational fluid dynamics code, to describe the behaviour of the various plasma species. Typical calculation results include the electrical characteristics (current, voltage, pressure relations), the electric field distribution, the densities, fluxes and energies of the various plasma species, information about the various collisions in the plasma and about cathode sputtering, optical emission intensities, etc. In this paper we focus on results that are of direct analytical interest, such as crater profiles and erosion rates due to sputtering, implantation profiles, glow discharge source design, optical emission intensities and the effect of hydrogen addition. Copyright © 2003 John Wiley & Sons, Ltd.

KEYWORDS: glow discharge; modelling; plasma; Monte-Carlo; fluid; crater profile; source design; optical emission spectrometry

INTRODUCTION

Glow discharges are used in various application fields,[1] ranging from the semiconductor industry and materials technology (deposition of thin films, etching and modification of surfaces) to lasers, light sources, plasma display panels, environmental and biomedical applications and analytical chemistry.[2–4] In the latter application the material to be analysed is typically a solid sample, although it is worth mentioning that increasing interest also exists for analysing samples in the liquid or gas phase.[5]

The glow discharge plasma is created by applying a potential difference between two electrodes that are placed in a cell (or they form the cell walls) filled with a gas. For analytical applications, argon is the most commonly used discharge gas at a pressure in the range 50–500 Pa. The potential difference is either constant in time (d.c. mode) or it can vary as a function of time (r.f. mode) or in the form of pulses (pulsed mode), and it is typically of the order of 1 kV. For the analysis of solid samples, the material to be analysed is typically used as the cathode (or r.f.-powered electrode) of the glow discharge, whereas the other cell walls are usually grounded. The argon glow discharge plasma consists of many different species, i.e. a large fraction of neutral atoms, as well as positive ions, electrons and excited species. The positive ions, as well as fast argon atoms created from argon ions, bombard the cathode and release atoms of the material to be analysed, which is called 'sputtering'. The sputtered, analytically important, atoms arrive in the plasma, where they are subject to collisions (mainly excitation and ionization) with the other plasma species. The ionization collisions create ions of the material to be analysed, which can be measured with a mass spectrometer (glow discharge mass spectrometry, GDMS), whereas the excitation collisions create excited species that emit characteristic photons that can be detected with glow discharge optical emission spectroscopy (GDOES). Furthermore, the sputtered atoms can be probed directly with external light sources for atomic absorption or fluorescence spectrometry (GDAAS and GDAFS), although these techniques are less common than GDMS and GDOES.

To improve the analytical capabilities of glow discharge sources, good insight into the plasma behaviour is desirable. We try to obtain this by numerical modelling. In the past decade we have developed a set of models to describe the behaviour of the various plasma species in an argon glow discharge with a copper cathode in d.c., r.f. and pulsed modes (see Refs 6–10 and references therein). In the present paper, we will give only a brief overview of the different models and then focus on the modelling results, which are of most analytical interest.

DESCRIPTION OF THE MODELING NETWORK

The analytical glow discharge under study operates in argon (Ar) as the discharge gas and the cathode (sample) is made of copper (Cu). The species assumed to be present in the glow discharge plasma include the (thermal) Ar gas atoms, fast Ar atoms, Ar atoms in various excited levels, Ar^+ ions, sputtered Cu atoms and the corresponding Cu^+ ions (in the

*Correspondence to: Annemie Bogaerts, University of Antwerp, Department of Chemistry, Universiteitsplein 1, B-2610 Wilrijk-Antwerp, Belgium. E-mail: annemie.bogaerts@ua.ac.be
Contract/grant sponsor: Flemish Fund for Scientific Research.

ground state and in various excited levels) and electrons. These species are described with a set of Monte-Carlo, fluid and collisional-radiative models, as well as a heat transfer model and a computational fluid dynamics code. The choice of the different models is based on the kinds of species to be described and their energy. Monte-Carlo models, which are very accurate but rather time consuming, are used for fast (energetic) plasma species that are not in equilibrium with the electric field (i.e. gain more energy from the electric field than they lose by collisions). Fluid models, which are faster but based on some approximations for hydrodynamic equilibrium, are applied for slow species for which these approximations are more or less valid. Collisional-radiative models are chosen for species in excited levels. Finally, a heat transfer model and a computational fluid dynamics code have been used for the Ar gas atoms. In the following, a brief overview of the different models will be given. We will not go into detail about the formulae used because they can be found in the cited references.

Fast electrons: Monte-Carlo model

The electrons are split into two groups, depending on their energy. The fast electrons, i.e. with total (sum of potential and kinetic) energy above the threshold for inelastic collisions, are treated with a Monte-Carlo model. Their trajectory, under the influence of the electric field, is calculated with Newton's laws during successive time-steps. Their collisions (occurrence of a collision, kind of collision and new energy and direction after collision) are treated with random numbers. A large number of individual electrons are followed in this way to obtain statistically meaningful results. More information about this model (formulae, collisions taken into account, cross-sections used, etc.) can be found in Refs 11 and 12. The electrons are followed until they are absorbed by the cell walls or until their energy drops below the threshold for inelastic collisions. In the latter case, the electrons are transferred to the slow electron group, to be treated with a fluid model (see below). Indeed, these slow electrons cannot give rise to inelastic collisions anymore; their only role is to carry electrical current and to provide negative space charge, which can be described also in a fluid model.

Slow electrons and Ar^+ ions: fluid model

The slow electrons are described in the fluid model with a continuity equation and a transport equation, based on diffusion and migration in the electric field. These two equations are coupled to similar continuity and transport equations for the Ar^+ ions, as well as to Poisson's equation. In this way, the electric field is calculated self-consistently, i.e. from the densities of the charged species calculated with the continuity equations. All these equations are strongly coupled, and solving this model is not a straightforward task. The solution method that we used is based on the Scharfetter–Gummel exponential scheme. For more information about this model (equations, input data, solution method, etc.) see Refs 12 and 13.

Note that usually we take only Ar^+ ions into account as positive ions, although we have developed a model in which the Ar_2^+ and Ar^{2+} ions were described.[14] Moreover, recently we have investigated the effect of H_2 on Ar glow discharges, and for this purpose the fluid model also takes the ArH^+, H^+, H_2^+ and H_3^+ ions into account as well as the Ar^+ ions.[15]

Fast Ar^+ ions and Ar atoms in the cathode dark space (CDS): Monte-Carlo model

Because the Ar^+ ions are in fact not in equilibrium with the electric field present in the cathode dark space (CDS), i.e. the region close to the cathode characterized by a strong electric field, they are described in this region not only with a fluid model but also with a Monte-Carlo model. Both models are in fact complementary, i.e. the fluid model calculates the Ar^+ ion densities self-consistently with the electric field distribution, whereas the Monte-Carlo model simulates the microscopic behaviour (e.g. collisions) of the ions and yields, among others, also the flux energy distribution needed to calculate sputtering at the cathode (see below). Note that it has been checked that both models yield the same calculation results for the fluxes and densities.

Apart from the Ar^+ ions, the fast Ar atoms created from the Ar^+ ions by collisions (i.e. energy transfer) with the Ar gas atoms are described with a Monte-Carlo model in the CDS. Indeed, it has been shown that the fast Ar atoms near the cathode play an important role in the analytical glow discharge, i.e. for sputtering and for ionization and excitation of the Ar gas.[11,16] These Monte-Carlo models for fast Ar^+ ions and Ar atoms in the CDS are described in detail in.[11,16]

Argon atoms in various excited levels: collisional-radiative model

The behaviour and populations of the Ar excited levels are calculated with a collisional-radiative model. Sixty-four excited levels are considered, most of them 'effective' levels consisting of several individual levels with similar quantum numbers and excitation energy. However, the four lowest levels (i.e. the 4s levels) are treated separately, because they play an important role in the analytical glow discharge. Indeed, two of them are metastable, i.e. they cannot decay radiatively to lower levels and therefore have a rather high population density and are very important for Penning ionization of the sputtered atoms. The other two levels can decay radiatively to the ground state but the emitted radiation is easily reabsorbed, leading again to excitation to the same 4s level. Hence, the two non-metastable 4s levels are also characterized by a rather high population density.

All excited levels are described with a balance equation, with various production and loss terms. The production and loss processes taken into account are all based on collisional and radiative mechanisms, hence the name of this model. They include excitation, de-excitation and ionization (from all levels) by collisions with electrons, Ar^+ ions and Ar atoms, electron–ion recombination to the excited atom levels, radiative decay between all levels, Hornbeck–Molnar associative ionization from the excited levels (yielding Ar_2^+) and some extra processes for the 4s levels (such as Penning ionization of the sputtered atoms, collisions between two 4s levels, two-body and three-body collisions with Ar gas atoms and transport by diffusion). All 64 balance equations

are coupled and solved simultaneously. More details about this model (e.g. processes considered, cross-sections used, etc.) are presented in Ref. 17.

Sputtering of the Cu cathode: empirical formula

Obviously, of most interest for analytical glow discharges is the sputtered material. The flux of sputtered Cu atoms is calculated by an empirical formula for the sputter yield as a function of bombarding energy,[18] multiplied by the flux energy distributions of the energetic species bombarding the cathode (i.e. Ar^+ ions, fast Ar atoms and Cu^+ ions), calculated in the Monte-Carlo models (see above and below).

Thermalization of the sputtered Cu atoms: Monte-Carlo model

When the Cu atoms are sputtered, they have typical energies of a few electron-volts. They lose this energy, however, rapidly by collisions with the Ar gas atoms until they are thermalized. This thermalization process is described with a Monte-Carlo model,[19] which yields the so-called thermalization profile, i.e. the number of thermalized sputtered atoms as a function of position from the cathode, which is used as input in the next model.

Copper atoms and ions in the ground state and excited levels: collisional-radiative model

Once the Cu atoms are thermalized, their further transport is diffusion-dominated. Moreover, the Cu atoms also can become ionized and/or excited. The behaviour of the Cu atoms and Cu^+ ions, both in the ground state and in various excited levels, as well as of the Cu^{2+} ions, is described with a similar collisional-radiative model as described above, which consists also of several balance equations (one for each level) containing different production and loss terms. The production and loss processes again include excitation, de-excitation and ionization from all levels, ion–electron recombination, radiative decay between all levels, Penning ionization of Cu by the Ar metastable atoms and asymmetric charge transfer between Cu atoms and Ar^+ ions. As mentioned above, transport of the Cu atoms is given by diffusion, whereas the transport of the Cu^+ ions is governed by diffusion and migration in the electric field. More details about this model (process, cross-sections, etc) can be found in Ref. 20.

Copper ions in the CDS: Monte-Carlo model

Similar to the Ar^+ ions, the Cu^+ ions are not in equilibrium with the strong electric field in the CDS either and they are therefore also described in this region with a Monte-Carlo model. This is indeed also important to obtain the flux energy distribution of the Cu^+ ions at the cathode, which plays a role in the sputtering (so-called 'self-sputtering').

Argon gas atoms: heat transfer model

Usually we assume that the Ar gas atoms are in thermal equilibrium at the gas temperature and we have no specific model to describe their behaviour. We simply assume in our models that the Ar gas atoms are uniformly distributed in the glow discharge plasma and their density (n) is calculated from the ideal gas law ($n = p/kT$), where the pressure (p) and gas temperature (T) are used as input in the model. However, experimental data for the gas temperature are not currently available. Therefore, we have also developed a model, based on the heat transfer equation, to calculate the gas temperature in the plasma as a result of gas heating due to collisions by energetic plasma species (fast Ar and Cu atoms and ions) with the Ar gas atoms.[21] This gives rise to a non-uniform temperature distribution (and hence density distribution) in the plasma.

Argon gas atoms: gas flow model

Apart from the effect of the non-uniform gas temperature distribution on the Ar gas density, the Ar gas can be non-uniformly distributed when there is a considerable gas flow in the glow discharge source. In most of our models described above, we do not consider a gas flow because in the glow discharge sources being studied the gas flow was assumed to be negligible. However, recently we have investigated the effect of the gas flow on our calculation results by coupling the above-described models to a computational fluid dynamics (CFD) code called 'Fluent', which describes the gas flow.[22] This CFD code yielded a non-uniform Ar gas density but the effect on the calculated density profiles of the other plasma species was found to be negligible. The fluxes of all plasma species (except the electrons), on the other hand, were significantly influenced by the gas flow because transport then is not only governed by diffusion (and migration for the charged species) but also by convection as a result of the gas flow (see later).

Coupling of the models

The above-described models are all coupled to each other by the interaction processes between the different plasma species, and they have to be solved iteratively (i.e. the output of one model is used as input in the next model, etc.) until convergence is reached. This takes typically several days on today's fast computers.

RESULTS OF THE MODELLING NETWORK

The modelling network has been applied in the past to various glow discharge sources (e.g. Grimm-type, VG9000 flat cell, pin-type cathode cell, six-way cross glow discharge cell), operation modes (d.c., r.f., pulsed) and discharge conditions (pressure, voltage, current). Because the investigated glow discharge cells can all be approximated as cylindrically symmetrical, all models (except the Monte-Carlo codes) are developed in two dimensions (i.e. axial and radial direction). The Monte-Carlo algorithms are fully developed in three dimensions, which was more straightforward and computationally no more difficult.

Typical modelling results include the electrical characteristics (current, voltage and pressure relations, also as a function of time, in the r.f. and pulsed mode), the electric field and potential distributions, the densities, fluxes and energies of the various plasma species, information about the various collisions in the plasma (e.g. relative contributions of the different production and loss processes for the various species), crater profiles and erosion rates as a result

of cathode sputtering, optical emission intensities due to radiative decay from the excited levels, etc. These results have been presented in the past in various papers (see Refs 6–10 and references therein). In the following, we will focus on results that are of direct analytical interest, such as surface analysis and depth profiling (crater profiles and erosion rates due to sputtering, Ar implantation profiles), glow discharge source design, optical emission intensities and the effect of H_2 on Ar glow discharges. The presented results have all been obtained for d.c. glow discharges, for which more experimental data were available as a check, but similar results also can be calculated with our models for r.f. and pulsed discharges.

Cathode sputtering

As mentioned above, the sputter flux is calculated from the flux energy distributions of the energetic plasma species bombarding the cathode, multiplied by the sputter yield, obtained from an empirical formula. The species playing a role in the sputtering (in an Ar discharge with Cu cathode) are the Ar^+ ions, the Cu^+ ions and the fast Ar atoms, created in the CDS from the Ar^+ ions. Figure 1 shows the calculated relative contributions of these species to the sputtering process as a function of voltage at different pressure values (typical for the VG9000 glow discharge ion source (a) and for a Grimm-type source (b)). The fast Ar atoms play the most important role for sputtering, especially at low pressures and low voltages. At high voltage and pressure, the Cu^+ ions become increasingly important and they were even found to have the dominant contribution in Grimm-type discharges at the highest voltages and pressures investigated. Finally, the Ar^+ ions are also rather important at all voltages and pressures investigated.

From the flux energy distributions of these species bombarding the cathode, calculated as a function of radial position, we can calculate the crater profile on the cathode after some time of sputtering. This is shown in Fig. 2(a) for a Cu cathode in the VG9000 glow discharge ion source at 1000 V, 3 mA and 75 Pa after 1 h of sputtering.[23] The calculated crater profile appears to be much deeper at the sides than in the centre, which is the result of the electric potential distribution in front of the cathode. The latter is presented in Fig. 3 for the same conditions as in Fig. 2(a). Note that the cathode (sample) is found at the left side of the figure, whereas the other figure borders are the cell walls at anode potential. The small black rectangles between $z = 0$ and 0.05 cm represent the insulating ring between cathode and anode, whereas the larger black rectangles between $z = 0.05$ and 0.15 cm stand for the 'front plate' of the cell, which is also at anode potential. The calculated potential is equal to −1000 V at the cathode and increases rapidly in the CDS. It goes through zero at ∼0.25 cm from the cathode and is slightly positive in the rest of the plasma, called the negative glow. It is clear from Fig. 3 that the equipotential surfaces in the CDS are not completely parallel to the sample surface, but they are bent in such a way that the ions (and also the atoms, which follow more or less the behaviour of the ions, from which they are created) are focused to

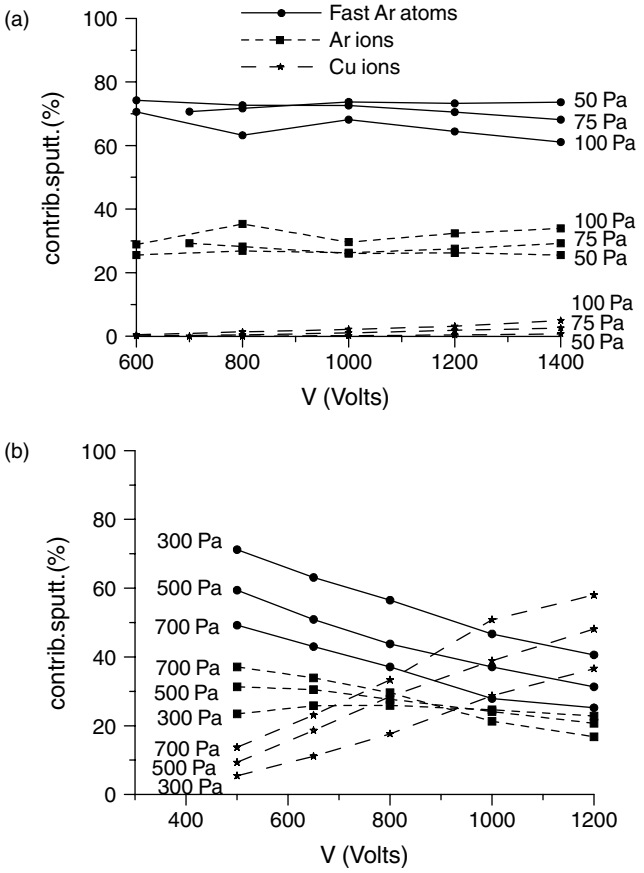

Figure 1. Calculated relative contributions of the Ar^+ ions, Cu^+ ions and fast Ar atoms to the sputtering process, as a function of voltage, at different pressures: (a) typical conditions of the VG9000 glow discharge ion source; (b) typical Grimm-type conditions.

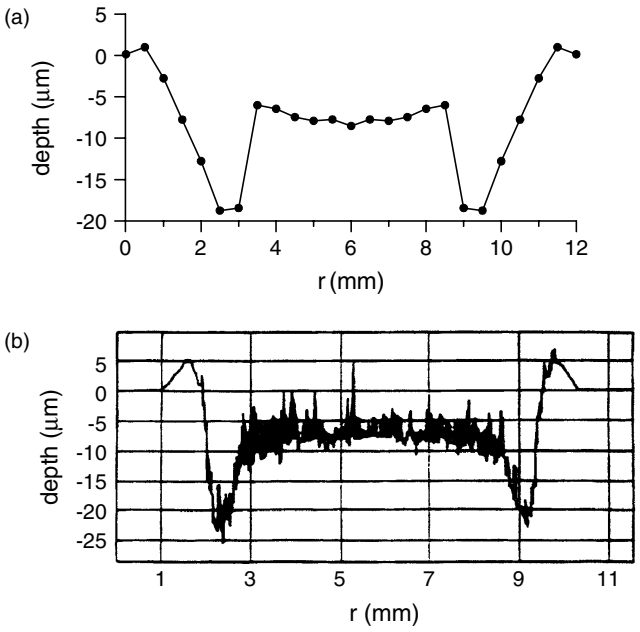

Figure 2. Calculated (a) and measured (b) crater profile after 1 h of sputtering in the VG9000 glow discharge ion source at 1000 V, 3 mA and 75 Pa. Reproduced from Ref. 23 with permission of Elsevier Science.

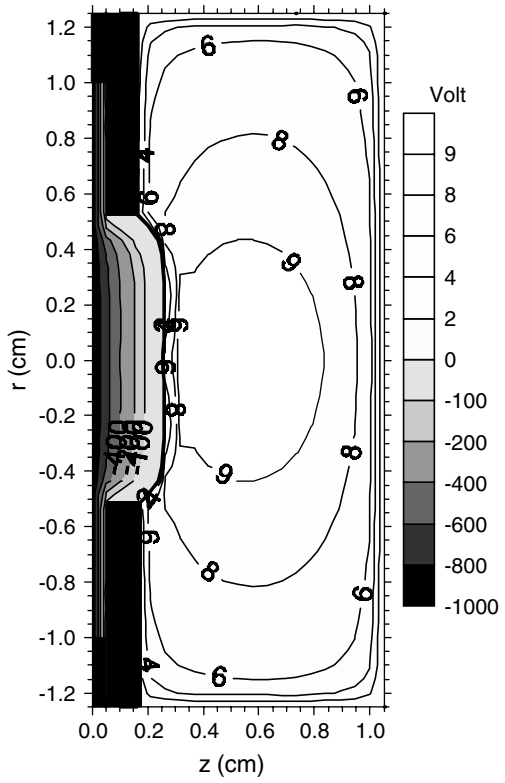

Figure 3. Calculated potential distribution in the VG9000 glow discharge ion source at 1000 V, 3 mA and 75 Pa. The cathode (sample) is found at the left side of the figure, whereas the other figure borders are the (anode) cell walls. The small black rectangles between $z = 0$ and 0.05 cm represent the insulating ring between cathode and anode, whereas the large black rectangles between $z = 0.05$ and 0.15 cm stand for the anode 'front plate'. Reproduced from Ref. 13 with permission of the American Chemical Society.

a distance of 0.3–0.4 cm from the cell axis, yielding more sputtering at these positions than in the centre.[23] Obviously, this crater profile is not very suitable for glow discharge depth profiling, because analyte atoms will be sampled from different depths (with possibly different compositions) at the same time, resulting in a bad depth resolution. However, this characteristic crater profile is also found experimentally, as is shown in Fig. 2(b), for the same conditions of voltage and current (the pressure could not be measured in this source).[23] Hence, this illustrates that the model can predict the characteristic crater profiles found experimentally with the VG9000 glow discharge ion source, and can elucidate the origin of this crater edge effect. Therefore, the modelling can be useful to predict how to eliminate this crater edge effect, e.g. by placing a mask in front of the sample or by modifying the cell geometry, particularly the position of the anode front plate, so that the equipotential surfaces can become parallel to the sample surface. In this way, the modelling can be useful for glow discharge source design.

Finally, it is worth mentioning that the measured crater profile (Fig. 2(b)) is also characterized by a small 'rim' outside the crater, which is also found, although not so pronounced, in our calculation result (Fig. 2(a)). This is attributed to redeposition of sputtered Cu atoms on the cathode, but outside the region where sputtering can take place (i.e. behind the anode front plate; cf. Fig. 3), so that there is a local rise in sputtered material instead of a loss.

Not only the cell geometry but also the discharge conditions (current, voltage, pressure) have a strong influence on the crater profile. Figure 4 illustrates calculated (a) and measured (b) crater profiles at constant voltage (but at different values of pressure and current) obtained for the VG9000 glow discharge ion source.[23] Both calculated and measured crater profiles change from a convex shape to a more flat shape at increasing pressure and current. The reason for this behaviour can be deduced from the modelling. Indeed, at higher pressure the CDS becomes shorter. Consequently, the zero potential surface (cf. Fig. 3) approaches closer to the cathode and the effect of the anode front plate becomes less pronounced, reducing the focusing of species towards the sides of the crater and hence resulting in a flatter crater.

By comparing the values at the y-axis of the calculated and measured crater profiles in Figs 2 and 4, it can be concluded that the modelling results are not only in good qualitative agreement with experiment but the calculated depths (or erosion rates) are in reasonable quantitative agreement with the experimental data. This has also been checked for the Grimm-type source. Figure 5 illustrates that the calculated erosion rates as a function of voltage at three different pressures in a Grimm-type source (solid lines) are in satisfactory agreement with the experimental data (dashed lines).[24]

Finally, beside the models for analytical glow discharges developed by ourselves, we have investigated the sputter process with a dynamic TRIM code called TRIDYN.[25] The TRIM code is based on a Monte-Carlo simulation of the interaction of ion beams with solid targets. The bombardment of an ion beam yields a cascade inside the target, which is treated as individual binary collisions. The TRIM code can be used to simulate both sputtering and deposition processes. More information about TRIM codes can be found in Ref. 26. We used a dynamic version, i.e. the TRIDYN code, which accounts for compositional changes in the target during the sputter process. It can simulate the change in composition of the target and the change of position of the surface (i.e. due to sputtering or deposition) as a function of time. Using the results from our modelling network (i.e. fluxes and average energies of the species bombarding the cathode) as input in TRIDYN, we studied the implantation of Ar inside a Cu target. Figure 6 presents the calculated implantation profile of Ar in the Cu target for the glow discharge conditions shown in Fig. 2, i.e. 1000 V, 3 mA and 75 Pa. For these conditions we calculated that the average energies of Ar^+ ions, fast Ar atoms and Cu^+ ions are in the order of 130 eV, 30 eV and 750 eV, respectively, and the fluxes of these species at the cathode are $\sim 2 \times 10^{16}$ cm^{-2} s^{-1}, 4×10^{17} cm^{-2} s^{-1} and 4×10^{15} cm^{-2} s^{-1}, respectively.[23] These data are used as input in the TRIDYN code. Moreover, the maximum concentration of Ar inside the target is set to 4%, i.e. the excess of Ar is assumed to diffuse out of the target. It appears from Fig. 6 that for the glow discharge conditions under study the Ar atoms can be implanted in the Cu target upto a depth of 30–40 Å. This is in reasonable correspondence with experimental data from Shimizu *et al.*,[27] who observed by

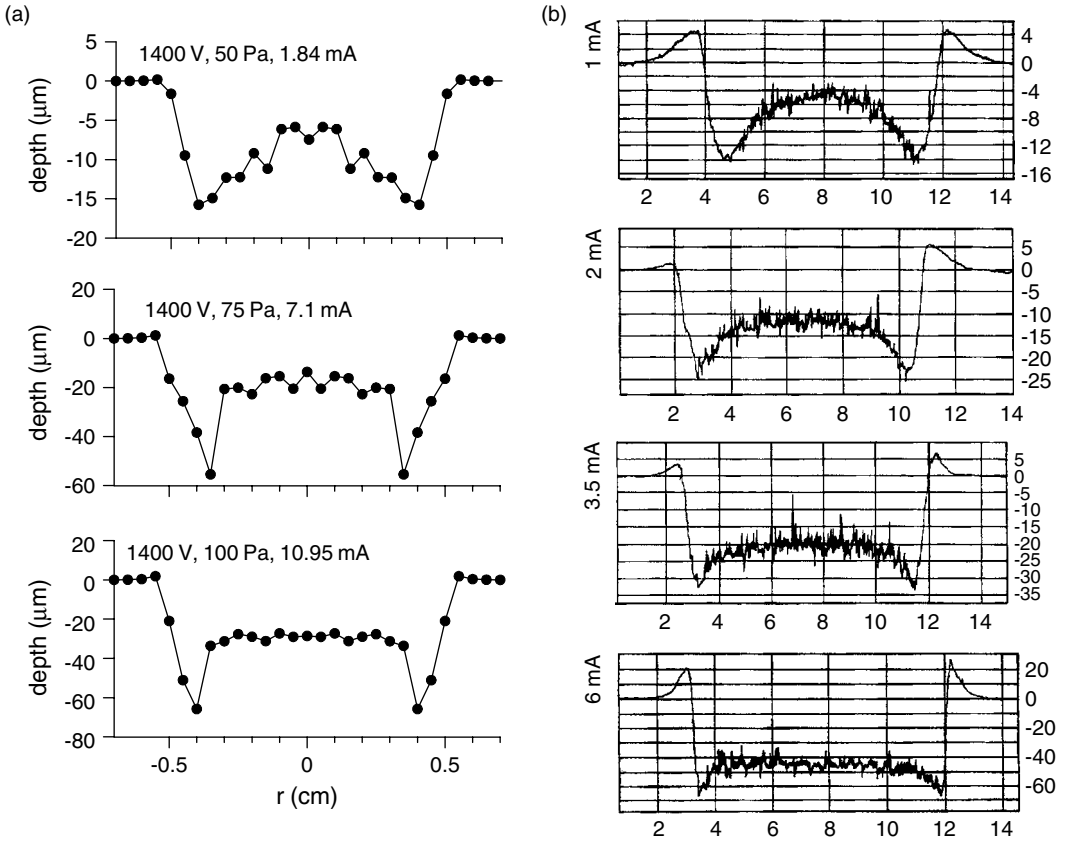

Figure 4. Calculated (a) and measured (b) crater profiles after 1 h of sputtering in the VG9000 glow discharge ion source at constant voltage but rising pressure and current. Reproduced from Ref. 23 with permission of Elsevier Science.

transmission electron microscopy a fine bubble-like texture, probably associated with implanted Ar, ''a few nm from the surface'' of an alumina film grown on aluminium that had been exposed to a glow discharge.

Optical emission intensities

Optical emission intensities can be calculated with our modelling network, more specifically with the collisional-radiative models for Ar atoms, Cu atoms and Cu^+ ions, based on the calculated level populations of the excited levels multiplied by the Einstein transition probabilities for radiative decay. We have compared the calculated emission intensities of several Ar and Cu lines as a function of voltage, at different pressures, with experimental data and reasonable agreement has been achieved.[24] Moreover, by comparing the calculated emission intensities, as a function of distance from the cathode, with experimental data we can check whether the correct processes are taken into account in our models.

Figure 7 shows the calculated (a) and measured (b) optical emission intensities of two Ar (I) lines, an Ar (II) line and a Cu (I) line as a function of distance from the cathode for different conditions of current and voltage.[28] The Ar (I) line at 750.38 nm (which originates from the $4p[1/2]_0$ level, i.e. a high 4p level) is characterized by a small peak near the cathode (i.e. in the so-called cathode glow), attributed to fast Ar^+ ion and Ar atom impact excitation, and a major peak in the beginning of the negative glow, due to electron impact excitation. On the other hand, the Ar (I) line at 811.5 nm (which originates from the $4p[5/2]_3$ level, i.e., a low 4p level)

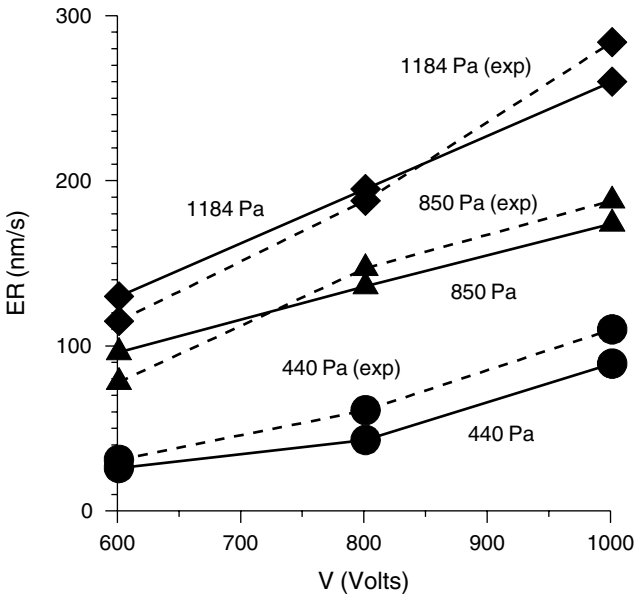

Figure 5. Calculated (solid lines) and measured (dashed lines) erosion rates in a Grimm-type source, as a function of voltage, at three different pressures. Reproduced from Ref. 24 with permission of Elsevier Science.

shows a pronounced peak in the cathode glow and a smaller peak in the negative glow. This suggests that the low 4p levels are predominantly populated by fast Ar^+ ion and Ar atom impact excitation, whereas electron impact excitation

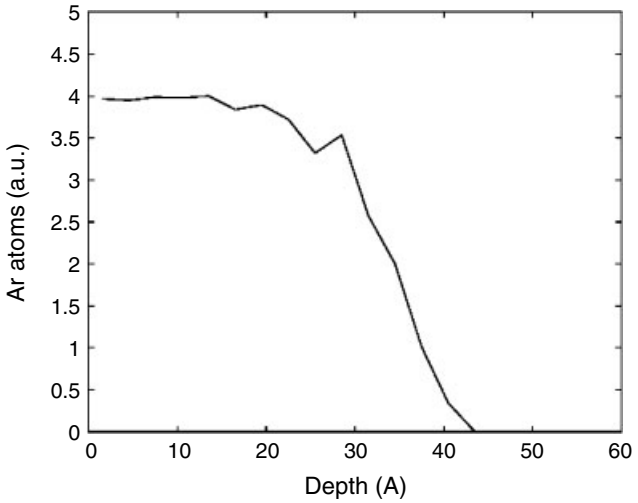

Figure 6. Calculated implantation profile of Ar in a Cu target for the VG9000 glow discharge ion source at 1000 V, 3 mA and 75 Pa. Note that the maximum concentration of Ar inside the target is set at 4%, i.e. the excess Ar is supposed to diffuse out of the target.

appears to be the most important production process for the high 4p levels. For still higher Ar levels, fast Ar^+ ion and Ar atom impact excitation are found to be negligible, because the energy required for efficient excitation of these levels is higher than the typical energies of fast Ar^+ ions and Ar atoms in the glow discharge. The same is true for the Ar^+ ion levels. Because we did not have enough input data available to develop a collisional-radiative model for the Ar^+ excited levels, we have simply calculated the Ar (II) line intensity of the 476.5 nm line based on electron impact excitation, yielding a maximum in the beginning of the negative glow. Finally, the intensity distribution of the Cu (I) 324.7 nm line is also characterized by a maximum in the beginning of the negative glow due to electron impact excitation. Moreover, the intensity of this Cu (I) line near the cathode is lower than for the Ar (I) and Ar (II) lines because the sputtered Cu atoms reach their maximum density at a few millimetres from the cathode. Our calculation results for these line intensities appear to be in very good agreement with the measured intensity distributions, as follows from a comparison of Figs 7(a) and 7(b). This demonstrates that the correct processes are described in our collisional-radiative models and that our models can, in principle, be useful for GDOES in order to make predictions on optical emission intensities.

Glow discharge source design

It has been discussed above that our modelling network can assist in glow discharge source design, e.g. to predict for which conditions and cell geometry a flat crater profile can be obtained, leading to a good depth resolution in glow discharge depth profiling. Also, we have applied our modelling network to hypothetical glow discharge cells with variable length and diameter[29] and with a flat-type or pin-type cathode.[30] Figure 8 illustrates the calculated Cu^+ ion density profiles in a cylindrically symmetrical glow

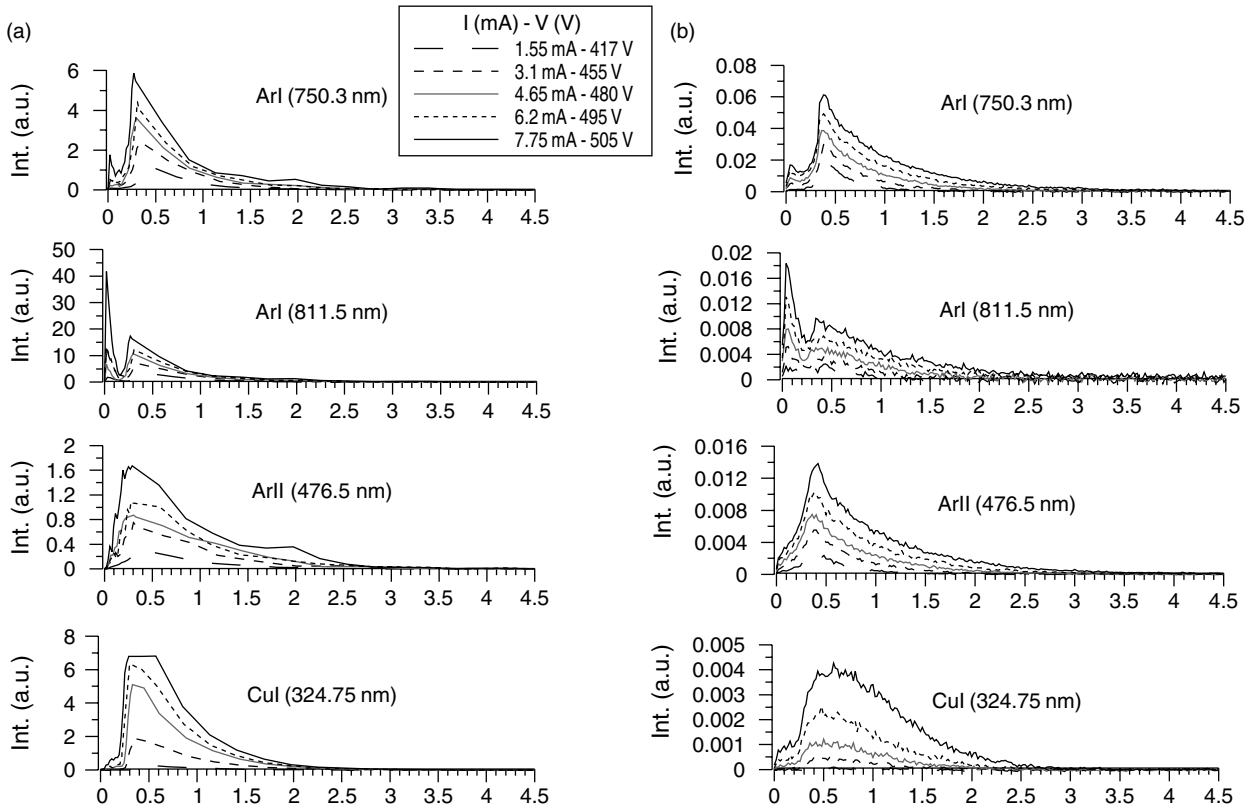

Figure 7. Calculated (a) and measured (b) optical emission intensities of two Ar (I) lines, an Ar (II) line and a Cu (I) line as a function of distance from the cathode for different conditions of voltage and current. Reproduced from Ref. 28 with permission of Elsevier Science.

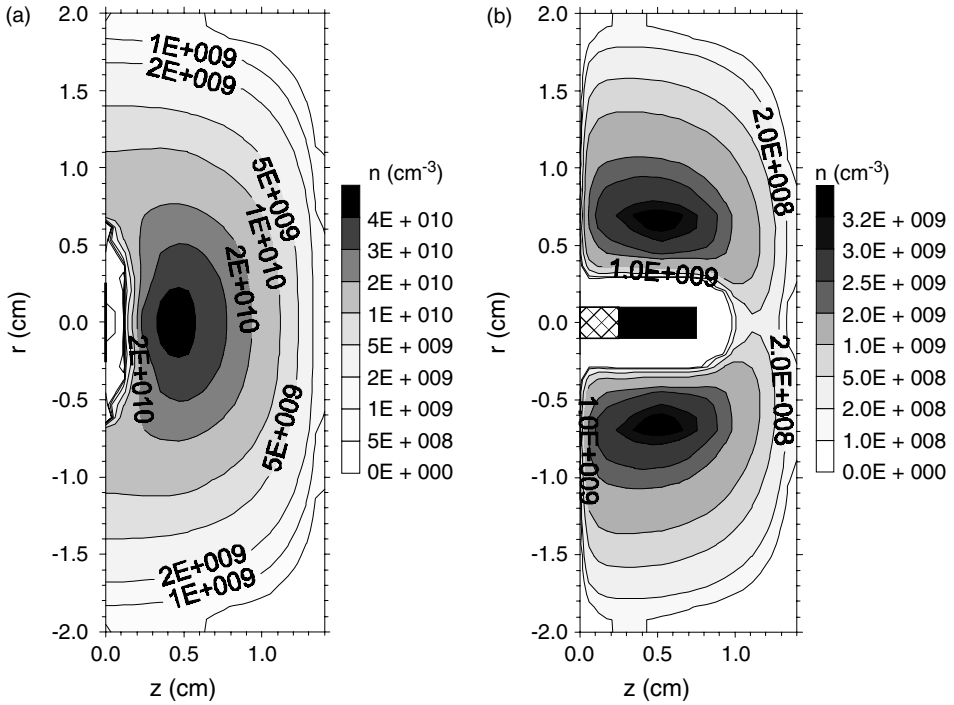

Figure 8. Calculated Cu^+ ion density profiles in a cylindrically symmetrical glow discharge cell with a flat cathode (a) and a pin cathode (b) at the same voltage and current (1000 V and 2.2 mA) but a different pressure (133 Pa for the flat cathode and 93 Pa for the pin cathode). Reproduced from Ref. 30 with permission of Elsevier Science.

discharge cell with a flat cathode (a) and a pin cathode (b). The comparison was made for the same voltage and current (1000 V, 2.2 mA) but in order to reach the same voltage and current the pressure in the pin cell was found to be lower than in the flat cell (i.e. 93 Pa vs 133 Pa).[30] The reason is that the pin cathode has a considerably larger area exposed to the discharge than the flat cathode, although the dimensions of both flat and pin cathode are comparable (i.e. diameter of flat cathode equals length of pin cathode = 5 mm) (see details in Ref. 30). Suppose that these glow discharge cells would be used as ion sources for GDMS, then the entrance slit to the mass spectrometer would be situated at the back end of the cell, probably at the cell axis. Note that from the Cu^+ ion density profiles information can be deduced about the ion fluxes towards this position of the entrance slit to the mass spectrometer, and hence one can have some idea about the Cu^+ ion peak intensities in the mass spectra.

In the flat cathode cell, the maximum Cu^+ ion density is reached at the cell axis ~5 mm from the cathode. In the pin cathode cell, the maximum density is located in a donut shape around the pin and the density between the top of the pin and the back end of the cell is much lower. Comparing the Cu^+ ion fluxes at the entrance slit to the mass spectrometer yields a value of 1.1×10^{14} cm^{-2} s^{-1} for the flat cell and a value of 9.1×10^{12} cm^{-2} s^{-1} for the pin cell under the conditions mentioned above. However, it should be realized that for these conditions the pressure in the pin cell is lower than in the flat cell. At a pressure of 133 Pa, the Cu^+ ion flux at the entrance slit of the mass spectrometer amounts to 4.5×10^{14} cm^{-2} s^{-1}, which is higher than the value in the flat cell. Hence, this shows that it is very difficult to compare the flat and pin cell under exactly the same conditions.

We have also investigated the influence of the sampling distance on the calculation results for both flat cells[29] and pin cells.[30] For the flat cell, the plasma species densities, the degree of ionization of Cu and the Cu^+ ion fluxes to the mass spectrometer appeared to increase for a rise in sampling distance from 0.5 to 2 cm, but a further rise in sampling distance did not result in an increase of the above calculated quantities.[29] A similar trend was also calculated for the pin cell, i.e. an increasing sampling distance (from 0.25 to 0.85 cm) yielded higher calculation results (e.g. higher plasma species densities and higher Cu^+ ion fluxes), which is in correlation with experimental observations from the literature.[31] Furthermore, at larger sampling distances the plasma species densities and Cu^+ ion fluxes (and hence analytical sensitivity) are expected to go over a maximum. Indeed, at short distances the plasma is somewhat restricted in place, and increasing the distance allows the plasma to spread out more throughout the cell and become more intense. However, at longer distances the plasma will not extend any further, and increasing the distance causes the cathode (source of sputtered analyte species) to be further away from the entrance slit of the mass spectrometer.[29,30] Although these are only theoretical predictions, we hope to have demonstrated that this type of modelling may be helpful for experimental source design.

As a last example of possible applications of the modelling network for glow discharge source design, we discuss here our recent modelling activities for the effect of the gas flow in a Grimm-type source.[22] Indeed, in recent developments for glow discharge ion source design for GDMS, a considerable gas flow is produced in the discharge to increase the ion transport towards the mass

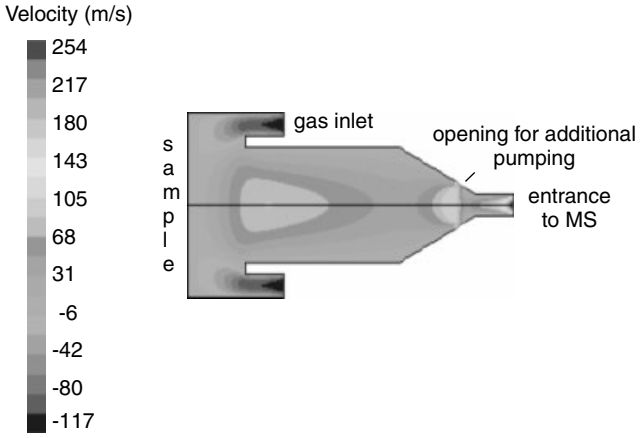

Figure 9. Calculated axial convection velocity of the Ar gas for an inlet flow rate of 100 sccm. Reproduced from Ref. 22 with permission of the Royal Society of Chemistry.

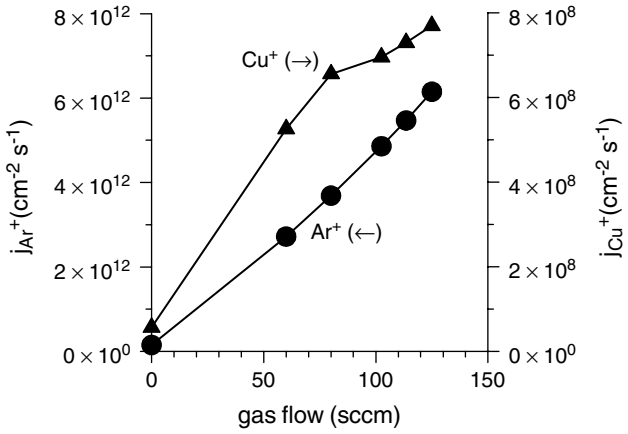

Figure 10. Calculated ion fluxes of Ar^+ (solid lines; left axis) and Cu^+ (dashed lines; right axis) at the entrance slit towards the mass spectrometer as a function of gas flow rate at 700 V and 60 mA. Reproduced from Ref. 22 with permission of the Royal Society of Chemistry.

spectrometer.[32] Figure 9 illustrates the axial convection velocity of the Ar gas, as calculated with the CFD program, for an inlet flow rate of 100 sccm. Note that a two-dimensional geometry was used, although the reality is three-dimensional at least for the gas injection. We have simulated the gas injection through a ring instead of a single opening; hence the (cylindrically symmetrical) calculation result does not entirely reflect reality, at least not in the immediate vicinity of the injection opening.

The gas flow is highly negative (i.e. directed towards the left) at the gas inlet position but in most of the cell geometry it is positive, i.e. directed towards the right (away from the cathode, towards the entrance of the mass spectrometer). It reaches its maximum value (i.e. several 100 m s^{-1}) at the exit to the mass spectrometer. As mentioned above, the gas flow was found to have a minor effect on the calculated density distributions of the various species, but the effect on the calculated fluxes was found to be very important (except for the electrons). Indeed, for the conditions under study (i.e. inlet gas flow rate ~100 sccm) convection was found to be the dominant transport mechanism in the negative glow and especially towards the end of the cell, with relative contributions of 70–90% to the total flux, for all plasma species except for the electrons.[22] Consequently, the ion fluxes of Ar^+ and Cu^+ ions at the entrance towards the mass spectrometer are calculated to increase significantly with rising gas flow rate, as is illustrated in Fig. 10. This is in reasonable qualitative agreement with experimental observations.[32,33]

Effect of H_2 on the Ar glow discharge

Recently, there has been increasing interest in the effects of small amounts of H_2 on the analytical results of Ar glow discharges.[34–37] It has been shown that some optical emission line intensities increase but others decrease when H_2 is added.[34,35] Also, the relative sensitivity factors (RSFs) of different elements in GDMS (which are a measure of the ionization efficiency) appear to be influenced by the addition of H_2.[36,37] Therefore, we have extended our modelling network to investigate the effect of H_2 on the Ar glow discharge. For this purpose a number of plasma species were added to the model, i.e. ArH^+, H^+, H_2^+, H_3^+, H and H_2, and in total 63 reactions were taken into account.[15]

Figure 11 shows the calculated densities of the various plasma species (taken at the maximum of their profile) as a function of H_2 addition to the Ar plasma.[38] The densities of the electrons, Ar^+ ions, Ar metastable atoms, sputtered Cu atoms and Cu^+ ions are found to decrease considerably as a result of H_2 addition, as is clear from Figs 11(a) and 11(b). A drop in electron and Ar^+ ion densities is also observed experimentally in the literature.[39] The reason for the drop in electron density is the recombination with ArH^+ ions and H_3^+ ions, whereas the drop in Ar^+ density is attributed to H-atom transfer of Ar^+ ions with H_2 molecules. The model predictions identify the reactions responsible for these effects, and these are in excellent agreement with experimental observations,[39] albeit for different discharge conditions. The calculated drop in Ar metastable atom density as a function of H_2 addition is due to collisions with H_2 molecules, leading to quenching of the Ar metastable level as well as excitation followed by dissociation of H_2. The latter is indeed found to be the most important mechanism for H_2 dissociation (and hence the formation of H atoms), which is in excellent agreement with experimental observations in the literature of a strong continuum emission in the spectral range of 220–440 nm, typically observed in $Ar–H_2$ glow discharges.[35] Because the Ar^+ ion and fast Ar atom fluxes bombarding the cathode, in analogy to the densities, also decrease with H_2 addition, the amount of sputtering drops and hence also the sputtered Cu atom density. Finally, the drop in Cu^+ ion density as a function of H_2 addition is due to a combination of a drop in Cu atom density and a drop in ionization efficiency of the Cu atoms. Indeed, the latter results from the lower Ar^+ ion and Ar metastable atom densities, leading to a drop in ionization of Cu atoms by asymmetric charge transfer with Ar^+ ions and Penning ionization by Ar metastable atoms (i.e. the two most important ionization mechanisms of Cu atoms). Electron impact ionization of Cu atoms also decreases slightly with H_2 addition, but the effect is less pronounced

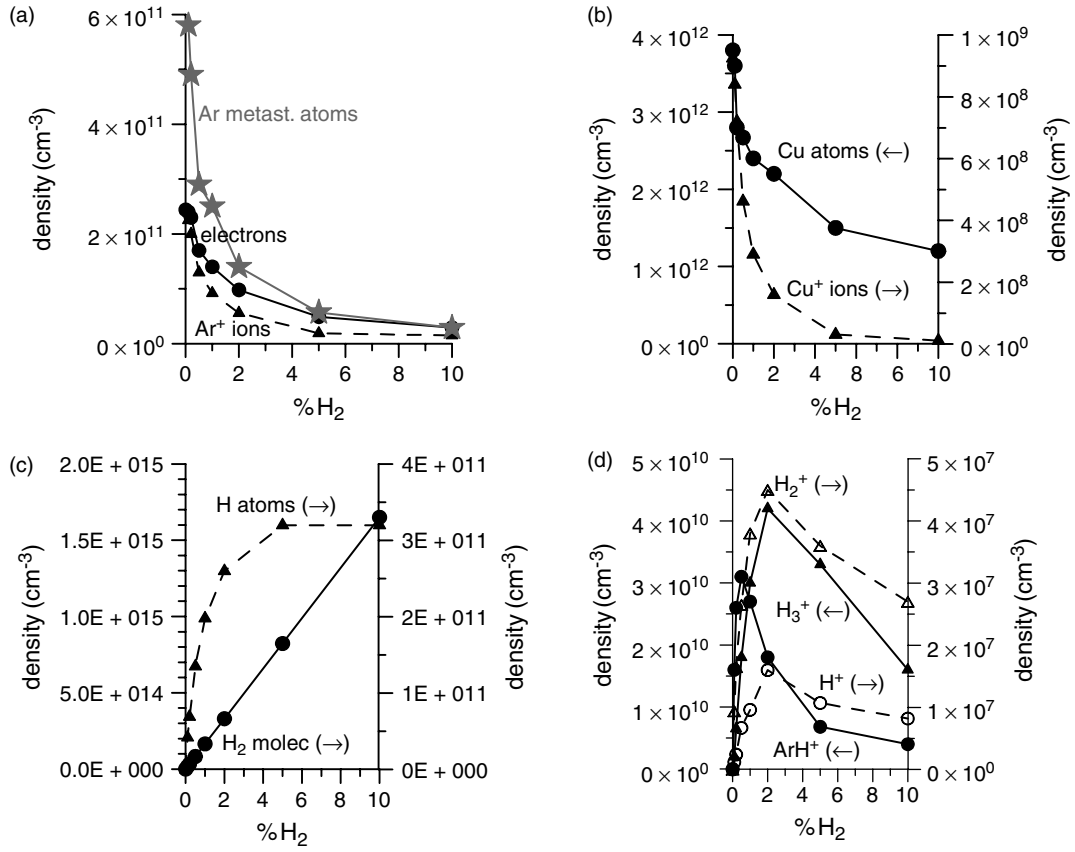

Figure 11. Calculated densities (at the maximum of their profiles) of electrons, Ar^+ ions and Ar_m^* metastable atoms (a), Cu atoms and Cu^+ ions (b) H_2 molecules and H atoms (c) and ArH^+, H^+, H_2^+ and H_3^+ ions (d) as a function of % H_2 addition at 1000 V, 3 mA and 75 Pa. Reproduced from Ref. 38 with permission of the Royal Society of Chemistry.

than for the other two ionization mechanisms. Hence, this means that the relative contributions of asymmetric charge transfer and Penning ionization drop,[38] whereas electron impact ionization becomes relatively more important. The latter can explain some observations in the literature, with respect to a better correlation between measured RSFs and values predicted by simple equilibrium models, based on the first ionization potential of the elements.[36,37] Indeed, the first ionization potential plays a role only in the electron impact ionization cross-section and not in the rate coefficients for Penning ionization and asymmetric charge transfer. Hence, this suggests indeed that electron impact ionization would be more important in the Ar–H_2 discharge than in the pure Ar discharge, which is at least qualitatively in accordance with our model predictions.

The densities of the H_2 molecules and H atoms rise as a function of H_2 addition (see Fig. 11(c)), as is expected. The effect is, however, less pronounced for the H atoms than for the H_2 molecules, resulting in a drop in the calculated degree of dissociation of H_2 with increasing hydrogen concentration. The densities of the hydrogen-related ions, i.e. ArH^+, H^+, H_2^+ and H_3^+, appear to pass over a maximum at a certain hydrogen concentration, which can be explained by the importance of the different production and loss mechanisms (see Ref. 38 for more explanation). The ArH^+ ions are formed by H-atom transfer between Ar^+ ions and H_2 (i.e. the major loss mechanism for Ar^+; see above), which explains the rather high ArH^+ density (e.g. calculated to be only a factor of 3 lower than the Ar^+ ion density, at 1% H_2 addition). Also, the H_3^+ ions have a rather high density at 1% H_2 addition (i.e. comparable to the ArH^+ density), which is attributed to the efficient proton transfer reaction between ArH^+ and H_2. The densities of H^+ and H_2^+ ions, on the other hand, are calculated to be several orders of magnitude lower. This calculation result of relatively high ArH^+ and H_3^+ ion densities and low H^+ and H_2^+ ion densities is also consistent with findings in the literature (see Ref. 38 for more details).

The above model predictions illustrate that our model can explain most of the effects observed experimentally in Ar–H_2 glow discharges. Hence, they provide a realistic picture of the role of H_2 in Ar glow discharges. Unfortunately, our model cannot yet predict the behaviour (rise or drop) of the optical emission line intensities as a result of H_2 addition. Indeed, this can be investigated only by comparing in detail the energy levels of H atoms and H_2 molecules with the energy level schemes of the elements concerned, because here a selective mechanism is expected to play a role (i.e. selective population or quenching of certain energy levels).

CONCLUSION

We have developed a comprehensive modelling network to describe the behavior of the various plasma species in an analytical Ar glow discharge with Cu cathode, including the effects of small amounts of H_2 addition. A large amount

of information can be obtained with these models, but we have focused here on the calculation results that are of direct analytical interest.

The calculated crater profiles and erosion rates as a result of sputtering are found to be in reasonable agreement with experimental data. The characteristic crater profile observed in the VG9000 glow discharge cell, which is not very suitable for depth profiling, could be backed up with our model; the origin of it could be clarified and some suggestions are made with respect to cell modification to improve the shape of the crater profile. Further, we have obtained information about the implantation depth of Ar in the Cu sample material using a Monte-Carlo code called TRIDYN.

Optical emission intensities of Ar and Cu atom and ion lines were also calculated with our model, and the excellent agreement with experimental data tells us that the correct processes are taken into account for the description of the excited levels and that the model can be useful in principle for GDOES in order to predict optical emission intensities.

We have also shown an example of our investigations on the effect of cell geometry on the calculation results. More specifically, we have presented a comparison between glow discharge cells with flat and pin cathodes and we have discussed the effect of sampling distance between the cathode and the entrance slit of the mass spectrometer. Moreover, we have investigated the effect of gas flow on the calculation results and it was shown that the fluxes of the various plasma species increase considerably with rising gas flow due to the important contribution of convection as a transport mechanism. The predicted increase of ion fluxes towards the mass spectrometer with rising gas flow was in qualitative agreement with experimental observations.

Finally, we have studied the effect of H_2 on Ar glow discharges. Most effects observed experimentally could be explained based on the importance of various collision processes in the plasma.

With the above examples, we hope to have illustrated that our modelling network can be useful to improve the analytical practice of glow discharges. Although the model is developed here for a Cu cathode, it can be applied to other materials as well, as long as the input data (e.g. sputtering yield, secondary electron emission coefficient, cross-sections for ionization and excitation, Einstein transition probabilities) are known.

Acknowledgements

A. Bogaerts is indebted to the Flemish Fund for Scientific Research (FWO-Flanders) for financial support. This research is also sponsored by the IUAP-V program. Also, we would like to thank W. Möller for supplying the TRIDYN code, V. Ignatova for help in its implementation, R. van de Sanden and the Eindhoven University of Technology for use of the CFD code and the computation time in the framework of a NATO SfP project, A. Okhrimovskyy for carrying out the Fluent calculations and Ch. Jonkers, V. Hoffmann and Z. Donko for supplying the experimental data.

REFERENCES

1. Bogaerts A, Neyts E, Gijbels R, van der Mullen JJAM. *Spectrochim. Acta B* 2002; **57**: 609.
2. Marcus RK. *Glow Discharge Spectroscopies*. Plenum Press: New York, 1993.
3. Payling R, Bengtson A, Jones D. *Glow Discharge Optical Emission Spectrometry*. John Wiley: Chichester, 1996.
4. Marcus RK, Broekaert JAC. *Glow Discharge Plasmas in Analytical Spectroscopy*. John Wiley: Chichester, 2003.
5. Bings NH, Bogaerts A, Broekaert JAC. *Anal. Chem.* 2002; **74**: 2691.
6. Bogaerts A, Gijbels R. *Anal. Chem.* 1997; **69**: A719.
7. Bogaerts A. *Plasma Sources Sci. Technol.* 1999; **8**: 210.
8. Bogaerts A, Gijbels R. *J. Anal. At. Spectrom.* 1998; **13**: 945.
9. Bogaerts A, Gijbels R. *J. Anal. At. Spectrom.* 2000; **15**: 1191.
10. Bogaerts A, Gijbels R. *J. Anal. At. Spectrom.* 2001; **16**: 239.
11. Bogaerts A, van Straaten M, Gijbels R. *Spectrochim. Acta B* 1995; **50**: 179.
12. Bogaerts A, Gijbels R, Goedheer WJ. *J. Appl. Phys.* 1995; **78**: 2233.
13. Bogaerts A, Gijbels R, Goedheer WJ. *Anal. Chem.* 1996; **68**: 2296.
14. Bogaerts A, Gijbels R. *J. Appl. Phys.* 1999; **86**: 4124.
15. Bogaerts A, Gijbels R. *Spectrochim. Acta B* 2002; **57**: 1071.
16. Bogaerts A, Gijbels R. *J. Appl. Phys.* 1996; **78**: 6427.
17. Bogaerts A, Gijbels R, Vlcek J. *J. Appl. Phys.* 1998; **84**: 121.
18. Matsunami N, Yamamura Y, Itikawa Y, Itoh N, Kazumata Y, Miyagawa S, Morita K, Shimizu R, Tawara H. *At. Data Nucl. Data Tables* 1984; **31**: 1.
19. Bogaerts A, van Straaten M, Gijbels R. *J. Appl. Phys.* 1995; **77**: 1868.
20. Bogaerts A, Gijbels R, Carman RJ. *Spectrochim. Acta B* 1998; **53**: 1679.
21. Bogaerts A, Gijbels R, Serikov VV. *J. Appl. Phys.* 2000; **87**: 8334.
22. Bogaerts A, Okhrimovskyy A, Gijbels R. *J. Anal. At. Spectrom.* 2002; **17**: 1076.
23. Bogaerts A, Gijbels R. *Spectrochim. Acta B* 1997; **52**: 765.
24. Bogaerts A, Wilken L, Hoffmann V, Gijbels R, Wetzig K. *Spectrochim. Acta B* 2001; **56**: 551.
25. Möller W, Eckstein W, Biersack JP. *Comput. Phys. Commun.* 1988; **51**: 355.
26. Biersack JP, Eckstein W. *Appl. Phys. A* 1984; **34**: 73.
27. Shimizu K, Habazaki H, Skeldon P, Thompson GE, Wood GC. *Surf. Interface Anal.* 1999; **27**: 950.
28. Bogaerts A, Donko Z, Kutasi K, Bano G, Pinhao N, Pinheiro M. *Spectrochim. Acta B* 2000; **55**: 1465.
29. Bogaerts A, Gijbels R. *J. Anal. At. Spectrom.* 1997; **12**: 751.
30. Bogaerts A, Gijbels R. *J. Am. Soc. Mass Spectrom.* 1997; **8**: 1021.
31. De Gendt S, Van Grieken R, Hang W, Harrison WW. *J. Anal. At. Spectrom.* 1995; **10**: 681.
32. Beyer C, Feldmann I, Gilmour D, Hoffmann V, Jakubowski N. *Spectrochim. Acta B* 2002; **57**: 1521.
33. Tanakia T, Kubota T, Kawaguchi H. *Anal. Sci.* 1994; **10**: 895.
34. Hodoroaba V-D, Hoffmann V, Steers EBM, Wetzig K. *J. Anal. At. Spectrom.* 2000; **15**: 951.
35. Hodoroaba V-D, Hoffmann V, Steers EBM, Wetzig K. *J. Anal. At. Spectrom.* 2000; **15**: 1075.
36. Smithwick IIIRW, Lynch DW, Franklin JC. *J. Am. Soc. Mass Spectrom.* 1993; **4**: 278.
37. Saito M. *Anal. Chim. Acta* 1997; **355**: 129.
38. Bogaerts A. *J. Anal. At. Spectrom.* 2002; **17**: 768.
39. Meulenbroeks RFG, van Beek AJ, van Helvoort AJG, van de Sanden MCM, Schram DC. *Phys. Rev. E* 1994; **49**: 4397.